Article

Temperature Dependent Crystal Structure of Nd$_2$CuTiO$_6$: An In Situ Low Temperature Powder Neutron Diffraction Study

N. Kumar [1], S. D. Kaushik [1], K. Sandeep Rao [2,3], P. D. Babu [1], S. K. Deshpande [1], S. N. Achary [2,3,*] and Daniel Errandonea [4,*]

[1] UGC-DAE Consortium for Scientific Research Mumbai Centre, Bhabha Atomic Research Centre, Mumbai 400085, India

[2] Homi Bhabha National Institute, Anushaktinagar, Mumbai 400094, India

[3] Chemistry Division, Bhabha Atomic Research Centre, Mumbai 400085, India

[4] Departamento de Física Aplicada-ICMUV, MALTA Consolider Team, Universidad de Valencia, Dr. Moliner 50, Burjassot, 46100 Valencia, Spain

* Correspondence: sachary@barc.gov.in (S.N.A.); daniel.errandonea@uv.es (D.E.)

Abstract: Herein we reported the crystal structure and crystal chemistry of orthorhombic perovskite type Nd$_2$CuTiO$_6$ in between 2 K and 290 K as observed from the in situ temperature-dependent powder neutron diffraction (PND) studies. It is observed that the cations in octahedral sites are statistically occupied, and the ambient temperature orthorhombic structure is retained throughout the temperature range of the study. Absence of any long-range magnetic ordering down to 2 K is confirmed by both low-temperature PND and magnetization studies. The lattice shows strong anisotropic thermal expansion with increasing temperature, viz. almost no or feeble negative expansion along the a-axis while appreciably larger expansion along the other two axes ($\alpha_b = 10.6 \times 10^{-6}$ K^{-1} and $\alpha_c = 9.8 \times 10^{-6}$ K^{-1}). A systematic change in the rotation of octahedral units with temperature was observed in the studied temperature range, while the expansion of unit cells is predominantly associated with the polyhedral units around the Nd^{3}Ions. The temperature-dependent relative change in unit cell parameters as well as coefficients of axial thermal expansion show anomalous behavior at lower temperatures, and that seems to be related to the electronic contributions to lattice expansion.

Keywords: perovskite; rare-earth compounds; thermal expansion; neutron diffraction; crystal structure; magnetic properties

1. Introduction

Perovskite-type materials are of interest due to their wide variety of functional properties, ranging from dielectric, ferroelectric, magnetic, and transport properties, as well as their structural diversity depending on composition and external thermodynamic parameters like temperature and/or pressure [1–3]. The structure, local distortion, and hence the properties of such perovskites are strongly dependent on the ionic radii and electronic configuration of the ions forming them [4,5]. Sequential structural transition in perovskites induced by chemical substitution, pressure, or temperature is a widely investigated topic of fundamental research in crystallography and materials science [4–8]. In general, the octahedral units of the perovskite structures behave as rigid units. However, depending on the ionic radii of other cations, these octahedral units may undergo distortion, ordering, or tilting in comparison to aristotype primitive cubic (*Pm3m*) type perovskite. Thus, the perovskite-type materials often exhibit sequential structural transformation with pressure, temperature, and composition [4,5]. Though geometrically such transitions are feasible, there are several cases where the transition to an undistorted and untilted structure is not observed, even up to the melting temperature. The ABO$_3$ type perovskites with A = rare-earth ions commonly crystallize in either a rhombohedral or orthorhombic structure depending on the nature and ionic radii of the rare-earth ions and octahedral site (B) cations [4,9–13].

Often the rare-earth perovskites show sequential structural transitions with temperature or pressure, and usually, the transformation sequence with increasing pressure is opposite to that observed with increasing temperature. The evolution of structural parameters with temperature or pressure often provides reasons for the presence or absence of phase transitions as well as an understanding of the nature and mechanism of the sequence of transitions [10–13].

In addition, the flexibility of composition and structural arrangement in perovskites render amenability to induce functionality for desired applications. Hence, the perovskite structures are considered prototypes for designing new materials with desired functional properties [1–3]. Several important functional properties like multiferroic and magnetodielectric properties have been observed in AMO_3 (A = rare-earth, M = transition metal ions like Fe, Mn, Cr, etc.) and $A_2MM'O_6$ (R = rare-earth or alkaline earth ions; M and M' = 3d transition metal ions) [3,6,14–17]. The rare-earth perovskites with Cu as an octahedral site ion show a wide range of physical properties like colossal permittivity, low dielectric loss, semiconducting behavior, and superconducting properties [8,18–27]. All such properties are invariably related to the oxidation state, local coordination, and distortion around the Cu ion. The influence of multiple oxidation states of Cu and Ti in La_2CuTiO_6 on the low-temperature transport phenomena was reported by Yang et al. [21]. Early experimental studies on La_2MTiO_6 (M = Co, Ni, Cu, and Zn) perovskites revealed cubic cation ordered lattices for M = Co, Ni, and Zn and a tetragonal lattice for M = Cu [28]. Through DFT calculations, Saha et al. predicted long-range antiferromagnetic ordering of the M^{2+} ions in cation ordered monoclinic La_2MTiO_6 (M = Co, Ni, and Cu) perovskites [25]. However, the recent studies on the low-temperature magnetic properties of Nd_2CuTiO_6 and La_2CuTiO_6 revealed no long-range magnetic ordering or cation ordering in both [21,23]. Further, several studies on La_2CuTiO_6 indicated no cation ordering in octahedral sites and structural or magnetic transition at low temperatures [21,22,24,27,29–31]. However, low-temperature heat capacity and magnetization measurements on Nd_2CuTiO_6 indicated a deviation in temperature-dependent heat capacity data, which was attributed to the spin reorientation of Cu and Nd [31]. Recently, we reported that the transport properties of Nd_2CuTiO_6 are strongly controlled by the valence states of Cu ions and associated oxygen vacancies [27]. As Cu^{2+} is a strong Jahn-Teller ion, it can be expected that the local coordination and distortion around Cu^{2+} can be altered by temperature. In order to understand the effect of temperature on the local surrounding around Cu, a detailed structural study on Nd_2CuTiO_6 was carried out using the in situ temperature-dependent powder neutron diffraction method. The magnetic measurements carried out under field and zero field cooled conditions indicated a noticeable difference in ZFC and FC magnetization curves at low temperatures. The evolution of structure from 2 K to ambient condition was followed by the variation of structural parameters with temperature. The analyses of structural parameters revealed an anisotropic expansion in the lattice, which could be attributed to the tilting of octahedral units with temperature. Further details of the temperature-dependent evolution of structural parameters of Nd_2CuTiO_6 are explained in the subsequent sections.

2. Materials and Methods

A polycrystalline sample of Nd_2CuTiO_6 was synthesized by a solid-state reaction route, as reported earlier [27] and it was characterized by powder X-ray diffraction. All the observed peaks in the XRD pattern could be assigned to the orthorhombic (*Pnma*) phase of Nd_2CuTiO_6 reported earlier (Figure S1, Supplementary Data) [27]. The powder neutron diffraction patterns of a Nd_2CuTiO_6 sample were recorded at different temperatures between 290 and 2 K using neutrons of wavelength 1.480 Å by employing the focusing crystal-based neutron powder diffractometer, PD3, at the Dhruva reactor, BARC, Trombay [32]. A finely ground sample was filled into a vanadium tube and capped tightly. The can was placed inside a CCR-based cryostat mounted on the PD3 beam line. The sample was cooled to 2 K and allowed to equilibrate for about 6 h, and then the diffraction data was collected. Subsequently, the temperature was raised to a desired value and then

equilibrated for 4 h prior to data collection. The analysis of all the neutron diffraction data was carried out by the Rietveld refinement method using the Fullprof-2 K software package [33]. Temperature-dependent magnetization of Nd_2CuTiO_6 was measured on a Vibrating Sample Magnetometer (VSM) attached to a Physical Property Measurement System (M/s. Quantum Design, San Diego, CA, USA) using an applied magnetic field of 100 Oe, and the isothermal magnetization measurements were carried out at 2.5 K. The temperature-dependent magnetization was measured in zero field cooled (ZFC) and field cooled (FC) modes. In the ZFC mode, the sample was cooled from room temperature to 2 K in the zero field, and a measuring field was applied at the lowest temperature. The magnetization was measured while heating the sample. After this run, the sample was cooled to the lowest temperature (2 K) in the presence of the field, and then the FC magnetization data was collected while warming the sample.

3. Results and Discussion

The structure of Nd_2CuTiO_6 was obtained by the Rietveld refinement of the powder neutron diffraction data recorded at 290 K. The structural parameters reported earlier from the powder XRD data [27] were used as the initial structural model for the Rietveld refinement. The Cu and Ti atoms are occupied in *4a* sites with a 0.5 occupancy each, while the Nd atoms are occupied in the *4c* sites of the space group *Pnma*. The oxygen atoms (O1 and O2) are occupied in the *8d* and *4c* sites. The background of the diffraction pattern was modelled by linear interpolation of selected points to create a smoothly varying background profile, while the profile of the Bragg peaks was generated using the Gaussian profile function. Initially, the scale, unit cell parameters, and profile function parameters were refined, and subsequently, the position coordinates and isotropic thermal parameters were included in the refinement. It may be mentioned here that no appreciable deviation of the occupancy of the oxygen atoms from stoichiometric Nd_2CuTiO_6 was observed. Thus, the occupancies of any atoms are not refined and are kept fixed according to their nominal stoichiometry. The good matching of the observed and calculated diffraction pattern is evidenced by the residuals of refinements (Rp = 3.96% and Rwp = 5.09%). A typical Rietveld refinement plot for the neutron diffraction data recorded at 290 K is shown in Figure 1. The refined structural parameters are given in Table 1.
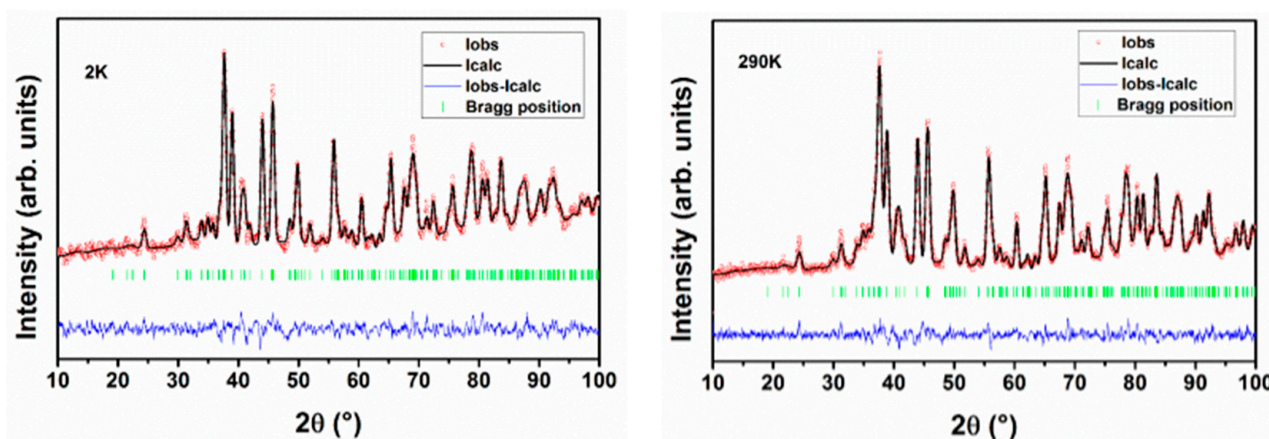

Figure 1. Rietveld refinement plots of powder neutron diffraction data recorded at 2 K and 290 K.

Table 1. Structural parameters of Nd_2CuTiO_6 at different temperatures.

	2 K	55 K	140 K	180 K	200 K	250 K	290 K
a (Å)	5.7283(5)	5.7282(4)	5.7263(5)	5.7262(1)	5.7274(5)	5.7270(4)	5.7277(4)
b (Å)	7.6160(6)	7.6160(6)	7.6201(7)	7.6236(6)	7.6288(6)	7.6304(6)	7.6393(5)
c (Å)	5.4568(4)	5.4550(4)	5.4575(5)	5.4616(5)	5.4649(4)	5.4678(4)	5.4723(3)
V (Å)^3	238.06(3)	237.98(3)	238.14(4)	238.42(4)	238.78(3)	238.94(3)	239.44(3)
Nd1							
4c (x, 1/4, z)							
x	0.5647(6)	0.5629(6)	0.5623(7)	0.5634(6)	0.5639(6)	0.5614(6)	0.5624(4)
z	0.0029(6)	0.0149(6)	0.0151(7)	0.0136(7)	0.0118(7)	0.0093(6)	0.0099(5)
B (Å)^2	0.19(5)	0.28(6)	0.32(6)	0.17(6)	0.22(6)	0.260(5)	0.25(4)
Occ.	1	1	1	1	1	1	1
0.5Cu/0.5Ti							
4a (0, 0, 0)							
B (Å)^2	0.23(19)	0.40(20)	0.28(23)	0.19(21)	0.03(21)	0.78(20)	0.88(16)
Occ.	0.5:0.5	0.5:0.5	0.5:0.5	0.5:0.5	0.5:0.5	0.5:0.5	0.5:0.5
O1							
8d (x, y, z)							
x	0.3060(6)	0.3013(6)	0.3021(8)	0.3027(6)	0.3032(6)	0.3012(6)	0.3013(5)
y	0.0460(4)	0.0458(4)	0.0458(5)	0.0458(4)	0.0461(4)	0.0456(4)	0.0450(3)
z	0.1979(6)	0.9096(7)	0.1971(7)	0.1984(6)	0.1972(6)	0.1987(6)	0.1988(4)
B (Å)^2	0.80(8)	0.46(8)	1.02(8)	0.79(7)	0.81(7)	0.94(6)	1.05(5)
Occ.	1	1	1	1	1	1	1
O2							
4c (x, 1/4, z)							
x	0.9752(6)	0.9755(6)	0.9748(8)	0.9762(7)	0.9746(7)	0.9760(6)	0.9756(5)
z	0.9151(7)	0.9096(7)	0.9084(8)	0.9149(8)	0.9148(8)	0.9114(7)	0.9112(6)
B (Å)^2	0.37(8)	0.46(8)	0.37(10)	0.45(10)	0.52(9)	0.49(8)	0.51(7)
Occ.	1	1	1	1	1	1	1
R_p, R_{wp}, χ^2	2.78, 3.52, 0.986	3.77, 4.77, 1.84	4.09, 5.10, 2.01	4.57, 5.75, 2.56	4.58, 5.16, 2.20	3.63, 4.62, 1.57	3.96, 5.08, 3.87
R_B, R_F	8.46, 6.98	5.16, 3.68	6.94, 4.79	6.49, 5.16	5.99, 4.58	4.98, 4.00	4.60, 3.02

The refined unit cell parameters of Nd_2CuTiO_6 at 290 K are: a = 5.7277(4) Å, b = 7.6393(5) Å and c = 5.4723(3) Å, which are comparable to the ambient temperature (300 K) unit cell parameters reported earlier [27]. The $(Cu/Ti)O_6$ octahedral units are formed with four O1 atoms (typical Cu/Ti-O1 distances are 2.069(3) Å × 2 and 2.032(3) Å × 2) and two O2 atoms (typical Cu/Ti-O2 distances are 1.976(1) Å × 2). These octahedral units are linked through O1 atoms along <101> directions and through the O2 atoms along <010> directions of the orthorhombic lattice. Different views of the crystal structure of Nd_2CuTiO_6 showing the $(Cu/Ti)O_6$ octahedra are depicted in Figure 2. The bond length distortion in the octahedral units is calculated from the observed bond lengths as $\Delta = \sum_{i=1}^{6} \frac{|d_i - \overline{d}|}{\overline{d}}$; where d_i is the length of the *i*th bond and $\overline{d}$ is the average bond length in polyhedra. The bond length distortion in $(Cu/Ti)O_6$ octahedra at 290 K is 3.58×10^{-4}. Similar analysis of the coordination polyhedra of the Nd atoms suggests that the Nd atoms are surrounded by eight oxygen atoms (six O1 and two O2 atoms) within distance limits of 2.65 Å. However, a conventional NdO_{12} polyhedral unit of perovskite structure can be visualized by considering additional two O1 and two O2 atoms at longer distances (Nd-O1 = 3.510(3) Å × 2, Nd-O2 = 3.404(4) Å and 2.207(4) Å, the bond length distortion being 242.8×10^{-4}). The angles (Cu/Ti)-O1-(Cu/Ti) and (Cu/Ti)-O2-(Cu/Ti) are 149.94 and 150.34°, respectively. The deviation of Cu/Ti-O1/O2-Cu/Ti from the regular 180° of an undistorted aristotype primitive cubic (*Pm3m*) ABO_3 lattice leads to the lower symmetric lattice for Nd_2CuTiO_6. The unit cell parameters of the orthorhombic (o) and undistorted cubic (*p*) lattices can be related as $a_o \sim \sqrt{2} \times a_p$, $b_o \sim 2 \times a_p$ and $c_o \sim \sqrt{2} \times a_p$. This can be explained by the $a^-b^+c^-$ Glazer tilt notation, where tilts of the octahedra are explained by three angles with respect to the aristotypic primitive cubic lattice, viz. θ from <110>$_p$, φ

from $<001>_p$ and Φ from $<111>_p$ axis, where subscript p indicates primitive *Pm3m* lattice. Since Φ is the result of the tilts θ and φ, only these two tilts are desired to explain the crystal structure of the orthorhombic *Pnma* structure. The tilts along different directions can thus also be quantified from the inert-octahedral bond angles, and subsequently, their variations provide the temperature and pressure responses on such perovskite-type materials. The values of tilts are thus obtained from the octahedral inter-polyhedral angles as per the relation given below [9,11], and the observed values of θ and φ at 290 K are 15.02° and 10.05°, respectively. The interatomic bond lengths and angles are given in Table 2.

$$cos\theta = cos\frac{\left[180 - \left\langle {}^{Cu}/_{Ti} - O1 - {}^{Cu}/_{Ti}\right\rangle\right]}{2} = cos^2\left|\varphi_x^-\right|$$

$$cos\varphi = \frac{cos\frac{\left[180 - \left\langle {}^{Cu}/_{Ti} - O2 - {}^{Cu}/_{Ti}\right\rangle\right]}{2}}{cos\left|\varphi_x^-\right|}$$

$$cos\varnothing = cos\theta \times cos\varphi$$

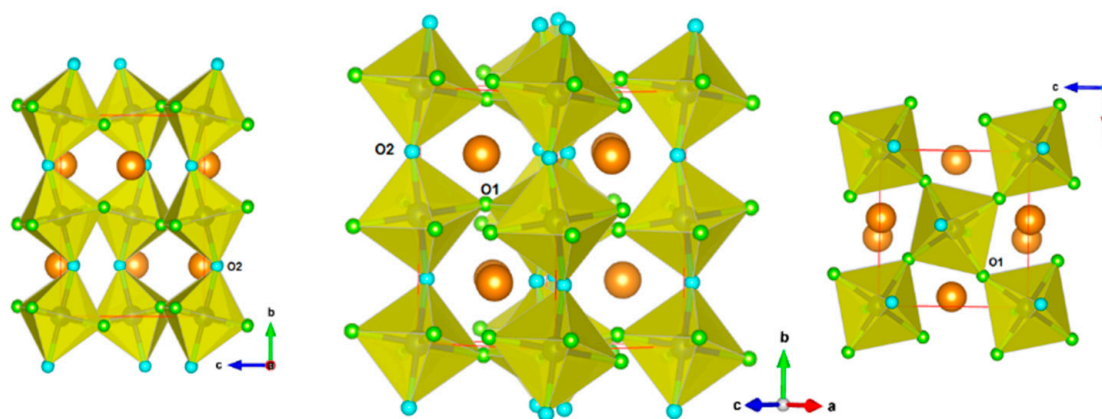**Figure 2.** Representation of the crystal structure of Nd_2CuTiO_6. $(Cu/Ti)O_6$ octahedral units are shown. The O1 and O2 are shown as small green and blue spheres, respectively. The larger brown spheres are Nd atoms.

Table 2. Interatomic bond lengths (Å) and angles (°) in Nd_2CuTiO_6 at different temperatures.

Bonds	2 K	55 K	140 K	180 K	200 K	250 K	290 K
Nd1-O1 × 2	2.396(4)	2.379(4)	2.372(5)	2.381(5)	2.382(5)	2.393(4)	2.400(3)
Nd1-O1 × 2	2.644(4)	2.596(4)	2.603(5)	2.603(5)	2.613(5)	2.620(4)	2.620(3)
Nd1-O1 × 2	2.614(4)	2.650(3)	2.650(4)	2.648(4)	2.643(4)	2.646(4)	2.644(3)
Nd1-O2	2.400(5)	2.432(5)	2.433(6)	2.424(5)	2.411(5)	2.434(5)	2.428(4)
Nd1-O2	2.338(5)	2.3691(5)	2.365(6)	2.392(6)	2.387(6)	2.352(5)	2.357(4)
CN	8	8	8	8	8	8	8
Av.Dis	2.506(2)	2.507(2)	2.506(2)	2.510(2)	2.509(2)	2.513(2)	2.514(1)
Distt	24.85×10^{-4}	22.81×10^{-4}	24.15×10^{-4}	21.76×10^{-4}	22.66×10^{-4}	23.62×10^{-4}	22.70×10^{-4}
Cu/Ti1-O1 × 2	2.088(3)	2.065(3)	2.067(4)	2.074(4)	2.074(4)	2.068(3)	2.0688(3)
Cu/Ti1-O1 × 2	2.019(3)	2.034(3))	2.034(4)	2.028(4)	2.033(4)	2.033(3)	2.032(3)
Cu/Ti1-O2 × 2	1.965(1)	1.972(1)	1.975(1)	1.966(1)	1.969(1)	1.973(1)	1.976(1)
CN	6	6	6	6	6	6	6
Av.Dis	2.024(1))	2.024(1)	2.025(1)	2.023(1))	2.025(1)	2.024(1)	2.026(1)
Distt	6.26×10^{-4}	3.65×10^{-4}	3.54×10^{-4}	4.72×10^{-4}	4.57×10^{-4}	3.73×10^{-44}	3.58×10^{-4}
M-O1-M	148.78(13)	149.57(13)	149.34(15)	149.45(15)	149.09(15)	149.81(13)	149.94(11)
M-O2-M	151.44(4)	149.86(4)	149.46(5)	151.48(4)	151.31(4)	150.42(4)	150.34(3)

In an analogous manner, the structural parameters of Nd_2CuTiO_6 at different temperatures were obtained by refining the corresponding temperature neutron diffraction data. In all the cases, the observed diffraction patterns could be explained by the orthorhombic structure. No additional peaks or split of peaks were observed in any diffraction pattern.

This indicates no structural transition or long-range magnetic ordering occurs down to 2 K, the lowest temperature of this study. The absence of long-range magnetic ordering is also confirmed by the low-temperature magnetic property studies explained subsequently. The refined unit cell parameters of Nd_2CuTiO_6 at 2 K are a = 5.7283(5) Å, b = 7.6160(6) Å and c = 5.4568(4) Å. It can be seen that the distortion in the unit cell increases on a lower temperature. The orthorhombicity observed at 290 K and 2 K are 0.023 and 0.024, respectively. A typical Rietveld refinement plot for the powder neutron diffraction pattern recorded at 2 K is shown in Figure 1. Refined unit cell parameters and other structural parameters observed at different temperatures are given in Table 1.

A comparison of unit cell parameters observed at different temperatures indicates no drastic difference in magnitude or trend at any temperature. The typical variations of unit cell parameters with temperature are shown in Figure 3a. A smooth and gradual change of the unit cell parameters due to temperature-induced lattice contraction is only observed on lowering the temperature. From the variation of unit cell parameters, the temperature dependencies are obtained by fitting with second-order polynomial relations, and the values of the coefficients are given in Table 3. Further, from the variation of unit cell parameters, it can be concluded that the variation of unit cell parameters with temperature are anisotropic, viz., the a-axis shows almost no variation with temperature and rather a feeble expansion with decreasing temperature. However, the other two axes (b- and c-) show appreciable contraction on with a reduction in temperature. In between 2 and 290 K, the coefficients of average thermal expansion ($\alpha_X = \frac{(X_{290K} - X_{2K})}{X_{2K}(290-2)}$, along the a, b, and c-axes are -0.40×10^{-6} K^{-1}, 10.63×10^{-6} K^{-1}, and 9.83×10^{-6} K^{-1}, respectively. The relative variation of the unit cell parameters with temperature shown in Figure 3b indicates that the b and c-axes have almost similar behavior compared to the a-axis.
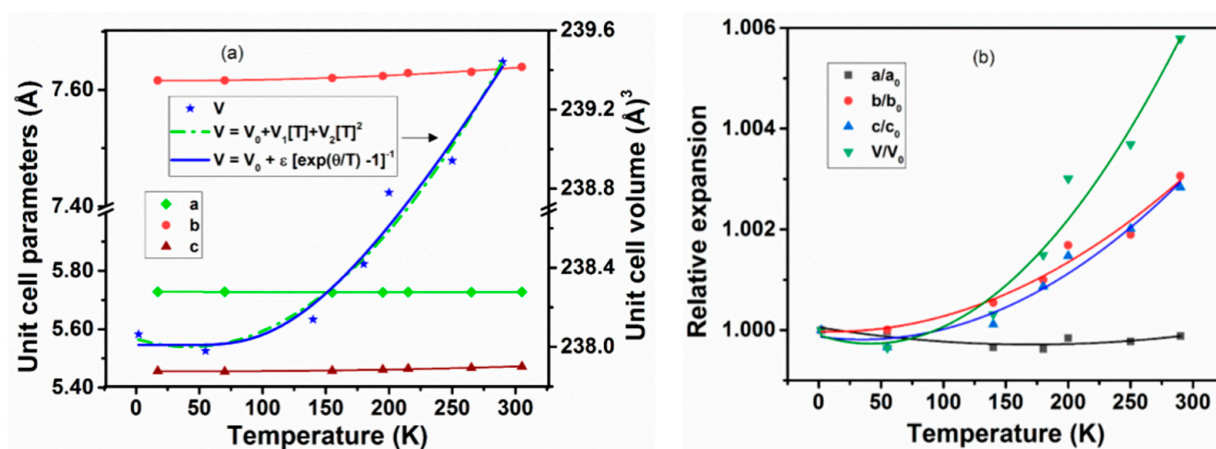

Figure 3. (**a**) Variation of the unit cell parameters of Nd_2CuTiO_6 with temperature. (**b**) The ratio of unit cell parameters with respect to their corresponding values at 2 K are plotted with temperature. Solid lines are second-order polynomial fits of temperature-dependent unit cell parameters. The temperature-dependent unit cell volume fitted with Einstein's expression of thermal expansion is shown as a solid blue line in the left panel.

Table 3. Coefficients of polynomial expression for the variation of unit cell parameters with temperature. $X(T) = X_0 + X_1 \times [T] + X_2 \times [T]^2$.

	a(Å)	b(Å)	c(Å)	V(Å)³
X_0	5.727(1)	7.616(1)	5.456(1)	238.0(1)
X_1	$-2.3(0.8) \times 10^{-5}$	$-0.6(2.4) \times 10^{-5}$	$-1.8(1.9) \times 10^{-5}$	$-0.002(2)$
X_2	$6.8(2.7) \times 10^{-8}$	$2.9(0.8) \times 10^{-8}$	$2.6(0.6) \times 10^{-7}$	$2.3(0.5) \times 10^{-5}$

In general, thermal expansion behavior at very low temperatures are not significantly contributed by the lattice vibrations, and hence often shows a saturation or noticeable expansion at low temperature. The temperature-dependent unit cell volume was fitted using the Einstein model of thermal expansion $V(T) = V_0 + \epsilon \left(e^{\frac{\theta}{T}} - 1\right)^{-1}$, where V is the unit cell volume, T is the temperature in K, ε is a constant, and θ is the characteristic Einstein temperature [34–38]. The fitting with the Einstein model shows a difference from the usual polynomial fits only at low temperatures. The fitted line is included in Figure 3a. The value of the Einstein constant ε depends on the bulk modulus and the Grüneisen parameter of the materials. The observed values of V_0, ε, and θ are 238.01 ± 0.08 Å^3, 5.7 ± 3.2, and $470 \pm 128K$, respectively. Besides, the temperature-dependent thermal expansion coefficients can be approximated by simpler polynomial relations, where the coefficients of the polynomials are limited by the considered range of temperature. The typical fit parameters are shown in Table 4, and the traces of temperature-dependent thermal expansion coefficients are shown in Figure 4. The coefficients of thermal expansion show a smooth increasing temperature dependence and no saturation until 290 K. The values of α_a, α_b, and α_c at 290 K are -0.4×10^{-6} K^{-1}, 10.6×10^{-6} K^{-1}, and 9.8×10^{-6} K^{-1}, while those at 55 K are -0.5×10^{-6} K^{-1}, 0.12×10^{-6} K^{-1} and -0.6×10^{-6} K^{-1}, and it is suggested that the behavior of the lattice expansion is temperature dependent, and, in particular, at low temperatures, its behavior is anomalous. This phenomenon is commonly observed in metallic and semiconducting materials [39–42].

Table 4. Coefficients of polynomial expression for the variation of coefficients of thermal expansion with temperature. $X(T) = X_0 + X_1 \times [T] + X_2 \times [T]^2$.

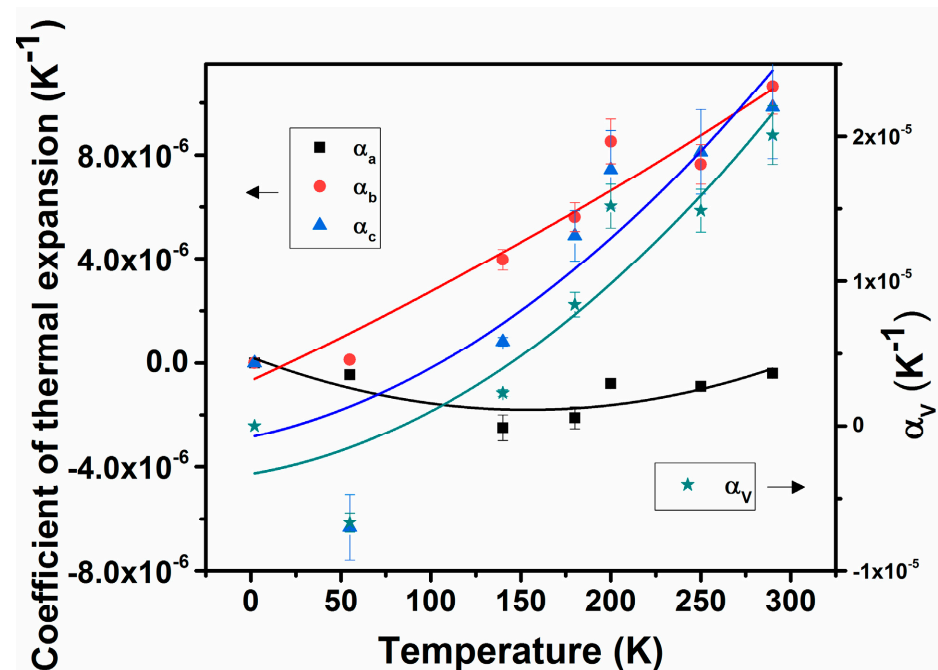|	α_a (K^{-1})	α_b (K^{-1})	α_c (K^{-1})	α_V (K^{-1})
X_0	$0.2(0.7) \times 10^{-6}$	$-0.7(1.1) \times 10^{-6}$	$-2.9(2.8) \times 10^{-6}$	$-3.3(3.8 \times 10^{-6}$
X_1	$-2.6(0.9) \times 10^{-8}$	$3.2(1.8) \times 10^{-8}$	$1.5(4.5) \times 10^{-8}$	$2.1(6.0) \times 10^{-8}$
X_2	$8.7(3.0) \times 10^{-11}$	$2.3(5.6) \times 10^{-11}$	$1.2(1.4) \times 10^{-10}$	$2.2(2.0) \times 10^{-10}$

Figure 4. Variations of coefficients of lattice thermal expansion with temperature.

The anomalous temperature-dependent thermal properties have also been reported for Nd_2CuTiO_6 from the heat capacity measurements, where a sudden increase in specific heat

on lowering the temperature below 10 K was observed [31]. The magnetic measurements were carried out on the present studied Nd_2CuTiO_6 sample to compare with the earlier reported data. The traces for temperature-dependent FC and FZC magnetization and field-dependent magnetization at 2.5 K are shown in Figure 5. In the present case, the magnetic measurements carried out at lower temperatures do not show any anomalous features, which rules out any long-range magnetic ordering. The difference in ZFC and FC behavior suggests short-range ordering or cluster formation in magnetic ions. The temperature-dependent magnetization shows typical paramagnetic behavior up to the lowest temperature. However, a separation between the ZFC and FC curves was noticed at ~3.2 K. This separation may be due to the short-range ordering of the magnetic ions. The M vs H curve shows a typical S-type curve with a feeble opening instead of a perfectly straight line expected for a paramagnetic material. The fast saturation and absence of any coercivity suggest a soft magnetic nature for Nd_2CuTiO_6. The analyses of temperature-dependent magnetic susceptibility at temperatures over 100–200 K indicated Curie-Weiss $\chi = \frac{C}{(T - \Theta_N)}$ type behavior with a negative Weiss temperature (-33.32 K). The negative Weiss temperature suggests a possible antiferromagnetic interaction in the sample. From the Curie constant, the effective magnetic moment per formula unit of Nd_2CuTiO_6 was calculated, and it is found to be 5.3 µB/FU. This is in agreement with the free ionic magnetic moment (J = S, spin only moment) of Nd^{3+} (3.46 µB) and Cu^{2+} (1.73 µB) [31,33] as expected by the relation $\mu_{eff} = \sqrt{\mu_{Nd3+}^2 + \mu_{Nd3+}^2 + \mu_{Cu2+}^2}) = 5.19$ µB/FU.

In order to compare the structures at different temperatures, it is convenient to express the orthorhombic lattices as primitive cubic structures using the relations explained earlier. The axial ratios, a_p:b_p:c_p for Nd_2CuTiO_6 at 290 K are 1.060:1.000:1.013 and those at 2 K are 1.064:1.000:1.013. These temperature-dependent axial variations in perovskite structures are the results of the tilting of $(Cu/Ti)O_6$ octahedra along the <101> and <010>. From the observed (Cu/Ti)-O1-(Cu/Ti) and (Cu/Ti)-O2-(Cu/Ti) bond angles at different temperatures, the values of tilt angle are obtained using the relation mentioned earlier. The variation of θ and φ with temperature is shown in Figure 6. It is observed that with decreasing temperature, the tilt angle (θ) shows an increasing trend, while the tilt angle (φ) shows a decreasing trend. Thus, the amplitude of octahedral rotation decreases along the $<110>_p$ of primitive cubic structure with increasing temperature, while that along $<001>_p$ has an opposite trend. Thus, a larger expansion along the b-axis results in the structure. Similarly, the increasing trend of rotation along $<111>_p$ of primitive structure is due to a combined effect of θ and φ, resulting in anisotropic expansion behavior along the a- and c-axes.

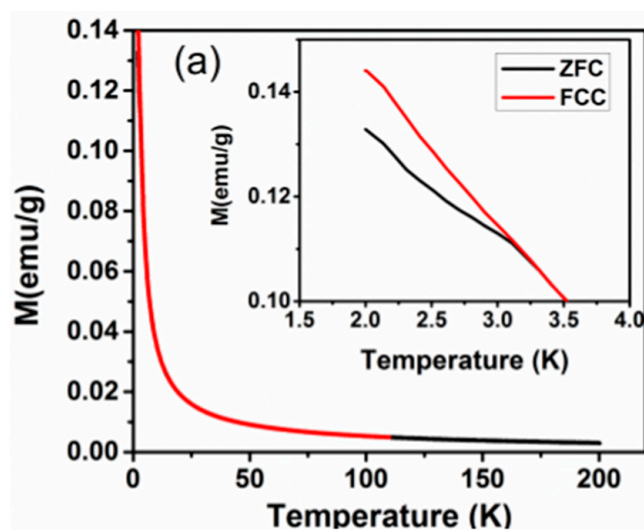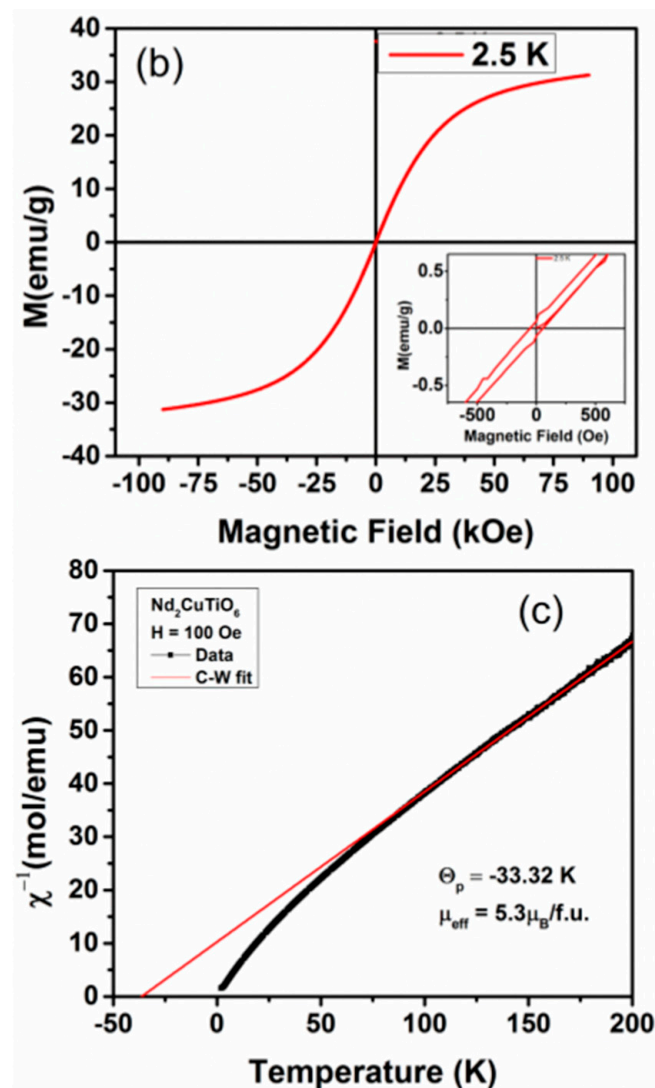**Figure 5.** *Cont.*

Figure 5. (**a**) ZFC and FCC M vs temperature plots of Nd_2CuTiO_6 sample in a field of 100 Oe. (**b**) M vs. H plot of Nd_2CuTiO_6. (**c**) Inverse magnetic susceptibility vs temperature plot of Nd_2CuTiO_6 sample and red solid line represent the Curie-Weiss law fitting.
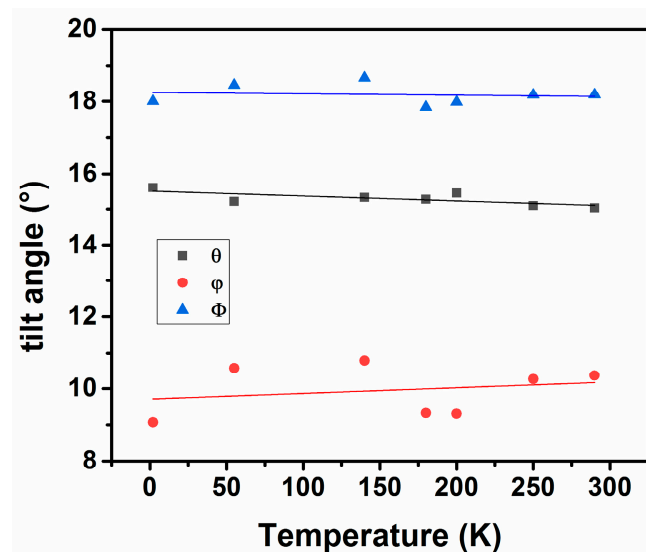

Figure 6. Variation of octahedral tilt angles in the structure of Nd_2CuTiO_6 with temperature.

Further, these tilts are reflected in the space inside the frame of octahedral units, which is occupied by Nd^{3+} ions, and that predominantly contributes to the lattice expansion of perovskite type structures. Thus, the polyhedra around the Nd^{3+} in the structure observed at different temperatures were analyzed. In the orthorhombic Nd_2CuTiO_6 lattice, Nd is displaced from the ideal positions of the perovskite structure and maintains an eight-coordinate polyhedron around it, while that has a regular twelve-coordinate polyhedron in an undistorted ideal structure. As explained earlier, the twelve coordinated NdO_{12} polyhedra can be constructed by including the oxygen atoms at longer distances (~3.5 Å). As expected, the bond length distortions $\left(\Delta_{NdO_{12}}\right)$ in NdO_{12} are significantly high at any temperature. The typical values $\Delta_{NdO_{12}}$ at 290 and 2 K are 242.8×10^{-4} and 252.3×10^{-4}, respectively, and an increasing trend with decreasing temperature is observed. The increase in symmetry and lowering of distortion in such a twelve-coordinate polyhedron often result the in transformation of lower symmetric structures into higher symmetric structures. The volumes of NdO_{12} and $(Cu/Ti)O_6$ polyhedral units at different temperatures are calculated from the structural parameters presented in Table 1, and the values are shown in Figure 7. An increasing trend in the volume of NdO_{12} and $(Cu/Ti)O_6$ units with increasing temperature from 2 K is observed. Commonly, the distortion in the AO_{12} unit governs the degree of anisotropy in the expansion or compressibility in the orthorhombic perovskite structure [12,34]. A systematically decreasing trend in the bond length distortion in NdO_{12} and an increasing trend in the volume of NdO_{12} polyhedra suggest a phase transition to a higher symmetric structure is expected only at higher temperatures. Further, it has been observed that the ratio of the polyhedral volumes of AO_{12} and BO_6 is a guiding factor for structural transition. In general, the orthorhombic structure remains stable when the ratio of AO_{12} and BO_6 remains higher than 3 [9–12,34], and, in the present cases, this ratio varied only marginally in the studied temperature range. Hence, the structure remains stable in this temperature range.
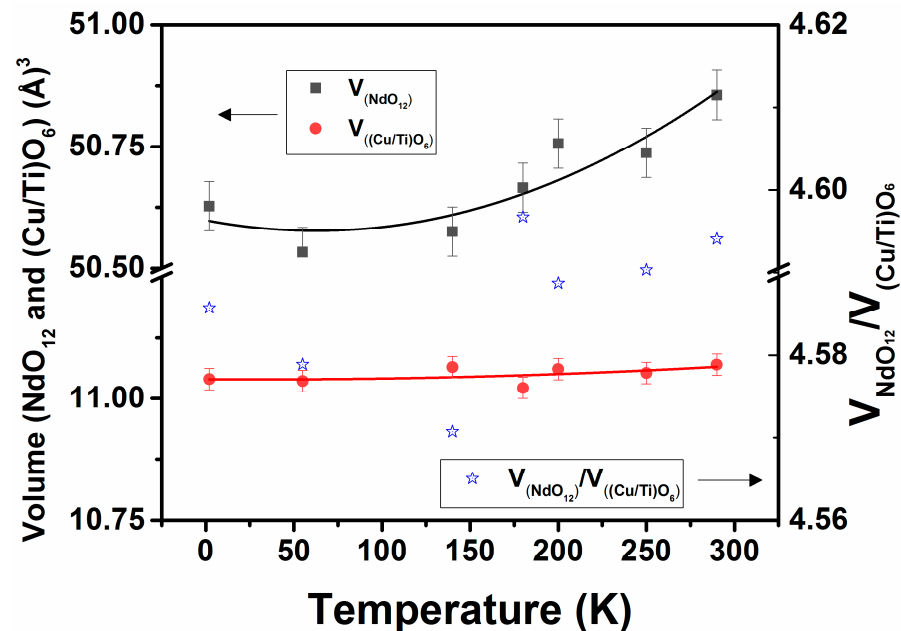

Figure 7. Variation of volume of NdO_{12} and Cu/TiO_6 polyhedra of Nd_2CuTiO_6 with temperature. $V_{NdO12} = 50.60(0.05) - 7.0(7.3) \times 10^{-4} \times [T] + 5.5(2.4) \times 10^{-6} \times [T]^2$; $V_{(Cu/Ti)O6} = 11.04(0.02) - 2.6(2.5) \times 10^{-5} \times [T] + 3.9(8.4) \times 10^{-7} \times [T]^2$, where T is temperature in K.

The analysis of structural parameters of Nd_2CuTiO_6 down to 2 K indicates that the contraction of unit cell parameters occurs mainly due to variation of inter-polyhedral angles. This is also reflected in the coordination polyhedra around the Nd^{3+} ions. At temperatures below 50 K, the lattice shows anomalous behavior with no or feeble negative expansion along the a- and c-axes. No long-range magnetic ordering is observed in the Nd_2CuTiO_6,

and magnetic moments corresponding to the free spin moments of the ions are observed over a wider range of temperatures. However, a possible antiferromagnetic interaction is evident from the negative Weiss temperature.

4. Conclusions

The evolution of the orthorhombic structure of Nd_2CuTiO_6 from 2 K to 290 K was delineated from the in situ variable temperature neutron diffraction studies. No cation ordering or magnetic ordering was observed from both neutron diffraction and magnetization studies. The structure showed anisotropic thermal expansion with larger expansion along the b-axis, while feeble negative expansion was observed along the a-axis in the studied temperature range. The anisotropy in expansion is related to the variation of the tilting of octahedral $(Cu/Ti)O_6$ units with temperature. The thermal expansion largely caused by the expansion and distortion of polyhedral around the Nd^{3+} ions. Besides, the studies also presented accurate structural parameters of Nd_2CuTiO_6 down to 2 K.

Author Contributions: Investigation, data curation, formal analysis, writing-original draft, N.K.; Investigation, data curation, formal analysis, writing-original draft, S.D.K.; Investigation, data curation, formal analysis, writing-original draft K.S.R.; conceptualization, writing-review and editing, validation, S.D.K.; conceptualization, writing-review and editing, validation, P.D.B.; conceptualization, writing-review and editing, validation, S.K.D.; conceptualization, writing-review and editing, validation, S.N.A.; conceptualization, writing-review and editing, validation, D.E. All authors have read and agreed to the published version of the manuscript.

Conflicts of Interest: The authors declare no conflict of interest.

References

1. Schaak, R.E.; Mallouk, T.E. Perovskites by design: A toolbox of solid-state reactions. *Chem. Mater.* **2002**, *14*, 1455.
2. Attfield, J.P.; Lightfoot, P.; Morris, R.E. Perovskites. *Dalton Trans.* **2015**, *44*, 10541–10542. [CrossRef] [PubMed]
3. Vasala, S.; Karppinen, M. $A_2B'B''O_6$ perovskites: A review. *Prog. Solid State Chem.* **2015**, *43*, 1–36. [CrossRef]
4. Glazer, A.M. The classification of tilted octahedra in perovskites. *Acta Cryst. B* **1972**, *28*, 3384. [CrossRef]
5. Howard, C.J.; Stokes, H.T. Group-Theoretical Analysis of Octahedral Tilting in Perovskites. *Acta Cryst. B* **1998**, *54*, 782–789. [CrossRef]
6. Achary, S.N.; Katari, V.; Sayed, F.N.; Tyagi, A.K. A brief review on the effect of preparation conditions on magnetic properties of some A_2MMnO_6 (A = La, Eu and Y; M = Mg, Co, Ni) type perovskites. *J. Chem. Sci.* **2019**, *96*, 131. [CrossRef]
7. Yin, W.-J.; Weng, B.; Ge, J.; Sun, Q.; Li, Z.; Yan, Y. Oxide perovskites, double perovskites and derivatives for electrocatalysis, photocatalysis, and photovoltaics. *Energy Environ. Sci.* **2019**, *12*, 442. [CrossRef]
8. Leo, A.; Motuzas, J.; Yacou, C.; Liu, S.; Serra, J.M.; Navarrete, L.; Drennan, J.; Julbe, A.; da Costa, J.C.D. Copper oxide—Perovskite mixed matrix membranes delivering very high oxygen fluxes. *J. Membr. Sci.* **2017**, *526*, 323. [CrossRef]

9. Martin, C.D.; Parise, J.B. Structure constraints and instability leading to the post-perovskite phase transition of MgSiO$_3$. Earth Planet. *Sci. Lett.* **2008**, *265*, 630–640.

10. Kennedy, B.J.; Vogt, T.; Martin, C.D.; Parise, J.B.; Hriljac, J.A. Pressure-induced orthorhombic to rhombohedral phase transition in LaGaO$_3$. *J. Phys. Condens Matter* **2001**, *13*, L925–L930. [CrossRef]

11. Dhak, P.; Pramanik, P.; Bhattacharya, S.; Roy, A.; Achary, S.N.; Tyagi, A.K. Structural phase transition in lanthanum gallate as studied by Raman and X-ray diffraction measurements. *Phys. Status Solidi B* **2011**, *248*, 1884–1893. [CrossRef]

12. Errandonea, D.; Santamaria-Perez, D.; Martinez-Garcia, D.; Gomis, O.; Shukla, R.; Achary, S.N.; Tyagi, A.K.; Popescu, C. Pressure Impact on the Stability and Distortion of the Crystal Structure of CeScO$_3$. *Inorg. Chem.* **2017**, *56*, 8363–8371. [CrossRef]

13. Rosas, B.Y.; Instan, A.A.; Mishra, K.K.; Achary, S.N.; Katiyar, R.S. Studies of Optical, Dielectric, Ferroelectric, and Structural Phase Transitions in 0.9[KNbO$_3$]-0.1[BaNi$_{1/2}$Nb$_{1/2}$O$_3$]. *Crystals* **2022**, *12*, 35. [CrossRef]

14. Rao, C.N.R.; Cheetham, A.K.; Mahesh, R. Giant Magnetoresistance and Related Properties of Rare-Earth Manganates and Other Oxide Systems. *Chem. Mater.* **1996**, *8*, 2421. [CrossRef]

15. Rogado, N.S.; Li, J.; Sleight, A.W.; Subramanian, M.A. Magnetocapacitance and Magnetoresistance Near Room Temperature in a Ferromagnetic Semiconductor: La$_2$NiMnO$_6$. *Adv. Mater.* **2005**, *17*, 2225. [CrossRef]

16. Tiwari, R.M.; Gadhvi, M.; Nag, A.; Vasanthacharya, N.Y.; Gopalakrishnan, J. Manganese-mediated ferromagnetism in La$_2$Fe$_{1-x}$Mn$_{2x}$Cr$_{1-x}$O$_6$ perovskite oxides. *J. Chem. Sci.* **2010**, *122*, 529. [CrossRef]

17. Dimitrovska-Lazova, S.; Aleksovska, S.; Tzvetkov, P. Synthesis and crystal structure determination of YCo$_{1-x}$Fe$_x$O$_3$ (x = 0, 0.33, 0.5, 0.67 and 1) perovskites. *J. Chem. Sci.* **2015**, *127*, 1173. [CrossRef]

18. Balachandran, N.; Robert, T.M.; Jayalatha, T.; Neema, P.M.; Mathew, D.; Cyriac, J. Lead-free, mixed tin-copper perovskites with improved stability and optical properties. *J. Alloys Compd.* **2021**, *879*, 160325. [CrossRef]

19. Zhao, J.; Chen, M.; Tan, Q. Embedding nanostructure and colossal permittivity of TiO$_2$-covered CCTO perovskite materials by a hydrothermal route. *J. Alloys Compd.* **2021**, *885*, 160948. [CrossRef]

20. Parrino, F.; García-López, E.; Marcì, G.; Palmisano, L.; Felice, V.; Sora, I.N.; Armelao, L. Cu-substituted lanthanum ferrite perovskites: Preparation, characterization and photocatalytic activity in gas-solid regime under simulated solar light irradiation. *J. Alloys Compd.* **2016**, *682*, 686. [CrossRef]

21. Yang, W.Z.; Mao, M.M.; Liu, X.Q.; Chen, X.M. Structure and dielectric relaxation of double-perovskite La$_2$CuTiO$_6$ ceramics. *J. Appl. Phys.* **2010**, *107*, 124102. [CrossRef]

22. Palacín, M.R.; Bassas, J.; Rodriguez-Carvajal, J.; Gomez-Romero, P. Syntheses of the perovskite La$_2$CuTiO$_6$ by the ceramic, oxide precursors and sol–gel methods, and study of the structure and Cu–Ti distribution by X-ray and neutron diffraction. *J. Mater. Chem.* **1993**, *3*, 1171. [CrossRef]

23. Gomez-Romero, P.; Palacin, M.R.; Casañ, N.; Fuertes, A.; Martinez, B. Towards the synthesis of layered perovskites. Synthesis, structure and magnetic properties of La$_2$CuTiO$_6$. *Solid State Ion.* **1993**, *603*, 63–65.

24. Zinenko, V.I.; Pavlovskii, M.S.; Shinkorenko, A.S. Electronic structure, lattice dynamics, and magnetoelectric properties of double perovskite La$_2$CuTiO$_6$. *Phys. Solid State* **2016**, *58*, 2294. [CrossRef]

25. Shah, S.; Ali, Z.; Mehmood, S.; Khan, I.; Ahmad, I. Electronic structure, optical and magnetic properties of double perovskites La$_2$MTiO$_6$ (M = Co, Ni, Cu and Zn). *Mater. Chem. Phys.* **2021**, *272*, 125050. [CrossRef]

26. Meng, L.; Feng, C.; He, L.; Deng, S.; Wu, Y.; Han, L.; Bai, Y. Understanding of the bond covalency nature with ionic electronegativity in perovskite cuprates La$_2$CuMO$_{6-x}$ (M = Ti, Mn, Ru). *J. Solid State Chem.* **2022**, *310*, 123050. [CrossRef]

27. Kumar, N.; Rao, K.S.; Sahu, A.K.; Deshpande, U.P.; Achary, S.N.; Deshpande, S.K. Role of oxygen partial pressure of synthesis environment in tuning the dielectric properties of Nd$_2$CuTiO$_6$. *Mater. Chem. Phys.* **2022**, *286*, 126203. [CrossRef]

28. Ramadass, N.; Gopalakrishnan, J.; Sastri, M.V.C. Preparation and characterization of La$_2$TiMO$_6$ (M = Co, Ni, Cu and Zn) perovskites. *J. Inorg. Nucl. Chem.* **1978**, *40*, 1453–1454. [CrossRef]

29. Singh, K.; Kumar, N.; Singh, B.; Kaushik, S.D.; Gaur, N.K.; Bhattacharya, S.; Rayaprol, S.; Simon, C. Magnetic and dielectric properties of R$_2$CuTiO$_6$ compounds (R = Y, La, Pr and Nd). *J. Supercond. Nov. Magn.* **2011**, *24*, 1829–1838. [CrossRef]

30. Rodriguez, E.; Lopez, M.L.; Campo, J.; Veiga, M.L.; Pico, C. Crystal and magnetic structure of the perovskites La$_2$MTiO$_6$ (M = Co, Ni). *J. Mater. Chem.* **2002**, *12*, 2798–2802. [CrossRef]

31. Rayaprol, S.; Kaushik, S.D.; Kumar, N.; Singh, K.; Guillou, F.; Simon, C. Neutron diffraction, specific heat and magnetization studies on Nd$_2$CuTiO$_6$ in Solid State Physics Symposium-2015. In *AIP Conference Proceedings*; American Institute of Physics: Melville, NY, USA, 2016; pp. 651–654.

32. Siruguri, V.; Babu, P.D.; Gupta, M.; Pimpale, A.V.; Goyal, P.S. A high resolution powder diffractometer using focusing optics. *Pramana, J. Phys.* **2008**, *71*, 1197–1202. [CrossRef]

33. Rodriguez-Carvajal, J. Recent advances in magnetic-structure determination by neutron powder diffraction. *Physica B* **1993**, *192*, 55–69. [CrossRef]

34. Mishra, A.K.; Garg, N.; Shanavas, K.V.; Achary, S.N.; Tyagi, A.K.; Sharma, S.M. High pressure structural stability of BaLiF$_3$. *J. Appl. Phys.* **2011**, *110*, 123505. [CrossRef]

35. Bevara, S.; Achary, S.N.; Mishra, K.K.; Ravindran, T.R.; Sinha, A.K.; Sastry, P.U.; Tyagi, A.K. Temperature dependent structural, vibrational and magnetic properties of K$_3$Gd$_5$(PO$_4$)$_6$. *Phys. Chem. Chem. Phys.* **2017**, *19*, 6030–6041. [CrossRef] [PubMed]

36. Chatterji, T.; Hansen, T.C. Magnetoelastic effects in Jahn–Teller distorted CrF$_2$ and CuF$_2$ studied by neutron powder diffraction. *J. Phys. Condens. Matter* **2011**, *23*, 276007. [CrossRef] [PubMed]

37. Achary, S.N.; Patwe, S.J.; Vishwanath, A.; Wajhal, S.; Krishna, P.S.R.; Tyagi, A.K. Evolution of crystal structure of PbMoO$_4$ between 5 and 300 K: A low temperature powder neutron diffraction study. *Mater. Chem. Phys.* **2021**, *260*, 124111. [CrossRef]

38. Tyagi, A.K.; Achary, S.N. Thermal expansion. In *Thermodynamic Properties of Solids*; Wiley-VCH Verlag GmbH & Co: Weinheim, Germany, 2010.

39. Atuchin, V.V.; Liang, F.; Grazhdannikov, S.; Isaenko, L.I.; Krinitsin, P.G.; Molokeev, M.S.; Prosvirin, I.P.; Jiang, X.; Lin, Z. Negative thermal expansion and electronic structure variation of chalcopyrite type LiGaTe$_2$. *RSC Adv.* **2018**, *8*, 9946–9955. [CrossRef]

40. Chimitova, O.D.; Bazarov, B.G.; Bazarova, J.G.; Atuchin, V.V.; Azmi, R.; Sarapulova, A.E.; Mikhailova, D.; Balachandran, G.; Fiedler, A.; Geckle, U.; et al. The crystal growth and properties of novel magnetic double molybdate RbFe$_5$(MoO$_4$)$_7$ with mixed Fe^{3+}/Fe^{2+} states and 1D negative thermal expansion. *CrystEngComm* **2021**, *23*, 3297–3307. [CrossRef]

41. Denisenko, Y.G.; Atuchin, V.V.; Molokeev, M.S.; Wang, N.; Jiang, X.; Aleksandrovsky, A.S.; Krylov, A.S.; Oreshonkov, A.S.; Sedykh, A.E.; Volkova, S.S.; et al. Negative thermal expansion in one-dimension of a new double sulfate AgHo(SO$_4$)$_2$ with isolated SO$_4$ tetrahedra. *J. Mater. Sci. Technol.* **2021**, *76*, 111–121. [CrossRef]

42. Achary, S.N.; Errandonea, D.; Muñoz, A.; Rodríguez-Hernández, P.; Manjón, F.J.; Krishna, P.S.R.; Patwe, S.J.; Grover, V.; Tyagi, A.K. Experimental and theoretical investigations on the polymorphism and metastability of BiPO$_4$. *Dalton Trans.* **2013**, *42*, 14999–15015. [CrossRef]